ISSN 2070-2051, Protection of Metals and Physical Chemistry of Surfaces, 2023, Vol. 59, No. 4, pp. 750–762. © Pleiades Publishing, Ltd., 2023.
ISSN 2070-2051, Protection of Metals and Physical Chemistry of Surfaces, 2023. © Pleiades Publishing, Ltd., 2023.

PHYSICOCHEMICAL PROBLEMS OF MATERIALS PROTECTION

Newly Synthesized Pyridinium Salt Based Tricationic Surfactants as Corrosion Inhibitor for Carbon Steel in 1.0 M HCl Medium

Serkan Öztürk[a], *, Gökhan Gece[b], Ayhan Yıldırım[a], and Hüsnü Gerengi[c]

[a] *Department of Chemistry, Faculty of Arts and Sciences, Bursa Uludag University, Bursa, 16059 Turkey*

[b] *Department of Chemistry, Faculty of Engineering and Natural Sciences, Bursa Technical University, Bursa, 16310 Turkey*

[c] *Corrosion Research Laboratory, Department of Mechanical Engineering, Faculty of Engineering, Düzce University, Düzce, 81620 Turkey*

**e-mail: serkanozturk@uludag.edu.tr*

Received November 7, 2022; revised April 26, 2023; accepted May 11, 2023

Abstract—Two pyridinium salt based tricationic surfactants were synthesized using quarternization reaction. The characterization of the surfactants were done by spectroscopic methods (FT-IR and NMR). Some pysicochemical properties like critical micelle concentration, surface tension at critical micelle concentration, Gibbs free energy of micelization, foam height, foam stability and emulsion stability were measured. The anticorrosion properties of the synthesized compounds were investigated by gravimetric measurements. In corrosion tests, where both compounds showed inhibitory activity against the corrosion of carbon steel in 1.0 M HCl environment, while the inhibition efficiency of the compound containing 6 carbon atoms in the long chain was determined in the range of 62–76%, those of the compound containing 8 carbon atoms in the long chain was found in the range of 85–93%. On the other hand, density functional theory (DFT) calculations were applied to arrive at basic molecular/electronic level scale details about the synthesized compounds, in addition to the surface images of the metal obtained by scanning electron microscopy to support the corrosion prevention results.

Keywords: synthesis, pyridinium, tricationic corrosion inhibitor, DFT, HCl medium

DOI: 10.1134/S2070205123700673

1. INTRODUCTION

Corrosion is a crucial problem that has not lost its importance until today. It causes irreversible problems, particularly in the metal industry. The concept of corrosion is used to describe the deterioration of metals and their alloys as a result of chemical and electrochemical reactions with their environment [1, 2]. In several industrial fields economical disadvantages occur via metallic corrosion [3]. Depending on the nature of the corrosive environment, the metals become unusable and this leads to a serious loss of efficiency. Metal deprivation by corrosion is a squander of not only the metal but also the dissipation, the water, and the human endeavour that was used to manufacture the metal structures at the outset [4]. One of the factors affecting the corrosion rate is the pH value of the environment. In general, the corrosion rate is high at low pH values, and does not change much at high pH values [5, 6].

Inhibitor utilization is the primary anti-corrosion method in acidic environments [7–9]. Inhibitors are substances added to the corrosion environments such as cleaning baths, cooling systems, various refinery units, chemical processes, steam generators, etc. to reduce or prevent the corrosive effect [10]. Specifically in acid cleaning industries, mineral acids (HCl, H_2SO_4 or H_3PO_4) are used, thus, the synthesis and use of organic inhibitors are highly substantial. As result of treatment with aqueous solutions of these acids, an oxide layer is often formed on the metal surface [11, 12]. These organic inhibitors, which passivate the metallic surface through the adsorption mechanism, change the electrochemical behavior of the medium in acidic solution and significantly reduce the aggressiveness of the acidic medium [13].

The use of surfactants has become inevitable for scientists working in the field of surface chemistry. Surfactant surveys is a fast moving field that makes ground in petroleum oil recovery, corrosion inhibition, water and environmental pollutions, biotechnology, and etc. [14]. These surfactants can be ionic (cationic, anionic), zwitterionic, or nonionic depending on the nature of their head groups [15]. Advanced inhibition efficacy, ruinous manufacturing expense, low toxicity and production facileness can be counted among the availments of surfactants. To control acid-induced corrosion, the use of organic cationic surfactants (mono- , di-, tri-) is the most efficient and prac-

tical method [16]. Surfactants adsorb to the metal surface, and accordingly, protect the metal against corrosion by reducing the corrosion rate in an acidic environment. The adsorption process onto the metallic surface in aqueous solution, to show the inhibitory action of surfactant molecules, can be physical (electrostatic interaction), chemical (donor-acceptor interaction) or mixed [8, 17, 18].

In recent years, cationic surfactants have come to the fore in corrosion inhibitor studies carried out in acidic environments. In some of these studies, it has been reported that mono-cationic surfactants [19–22] and in others di-cationic surfactants [23–28] act as corrosion inhibitors in acidic environment. In all of these studies, the inhibitory efficiency increased as the inhibitor concentration increased, as expected. In the literature, there are examples of studies in which tricationic surfactants are used as corrosion inhibitors in acidic environments [29–33], but their number is very few compared to mono- and di-cationic ones. On the other hand, there are studies on pyridinium salts, in which pyridine nitrogen is positively charged, as effective inhibitors against corrosion in acidic environments [34, 35]. In these studies, it was reported that pyridinium salts showed better inhibitory activity than quaternary ammonium salts due to the π electrons in the pyridine ring. Those π electrons interact with the vacant d orbitals of the metal atom on the surface and make an additional contribution to the adsorption. In this way, the surfactant adheres better to the surface and protects it against corrosion in the acidic environment [34, 35].

DFT-based computational studies have enabled improvements in inhibition efficiency prediction of corrosion inhibitors, and our conceptual view of inhibition mechanisms has been transformed in the past twenty years [36]. Although finding common ground among the molecular parameters and corrosion efficiency of a compound remains an elusive goal, such approaches highlight how far much further we have to go to develop sufficiently accurate estimation of the inhibition behaviour of the compounds [37].

In this study, two tricationic surfactants, with two positively charged pyridine nitrogens and one quaternary ammonium nitrogen on its structure, were synthesized. The critical micelle concentrations, surface tensions, foam properties and emulsion stability of these two surfactants with different carbon chains were determined and their effectiveness against corrosion of low carbon steel in 1.0 M HCl solution were compared. In order to support the inhibition results and to compare the roughness of the surface, images of the metal surface taken by scanning electron microscope (SEM) were obtained. In addition, quantum calculations were carried out in order to tackle the question of how pertinent molecular electronic parameters are for predicting the inhibition efficiency of those two tricationic surfactants.

2. EXPERIMENTAL

2.1. Solutions and Instrumentation

Reagents and solvents, namely, thionyl chloride, toluene, corresponding bromoalkanoic acids (C_6 and C_8), pyridine, 2-aminopyridine, ethanol and hydrochloric acid (HCl, 37%) were purchased from Merck (Merck, Darmstadt, Germany) and used without further purification. The other chemicals, namely, dichloromethane (CH_2Cl_2), triethylamine, (2-bromoethyl)trimethylammonium bromide were purchased from Sigma-Aldrich company (St. Louis, MO, USA). Thin layer chromatography (TLC) was performed using silica gel (60 F254, Merck, Darmstadt, Germany) plates. The FT-IR spectra of the tricationic surfactants synthesized as the final product were obtained with the Perkin Elmer Spectrum 100 (Shelton, Connecticut, USA) FT-IR spectrophotometer. ^{1}H NMR and ^{13}C NMR spectra were measured using Agilent 600 MHz Premium Compact NMR spectrometer (Santa Clara, CA, USA) in DMSO-d_6 using TMS as the internal standard. NUVE EV 018 vacuum oven (Ankara, Turkey) was used to dry the metal coupons until they reach constant weight. The elemental analyses were performed using an LECO CHNS-932 elemental analyzer (Saint Joseph, MI, USA).

2.2. Synthesis of Compounds

The syntheses of 6-bromohexanoyl chloride and 8-bromooctanoyl chloride were performed for 6 h refluxing using $SOCl_2$ in toluene. The acquired oily product was used without further purification in the step where the amidation reaction was ensued using 2-aminopyridine in dichloromethane for overnight in the presence of triethylamine (compunds **1a-b**). In the next step, **1a-b** were refluxed with pyridine in ethanol for 24 h. The solvent was blown off and the residue was elutriated with petroleum ether. After treatment with petroleum ether the beige solid (**2a-b**) were obtained. In the last step, the mixture of **2a-b** with (2-bromoethyl)trimethylammonium bromide and 20 mL of ethanol was refluxed for 48 h. Ethanol was blown off, and the extraction of the residue by acetone was achieved upon heating. The acetone extract was unmingled, and the solvent was evaporated to give an oily-solid wax product (**3a-b**).

2.2.1. 2-(4-(1-pyridinium-1-yl)hexanamido)-1-2-(trimethylammonio)ethyl)pyridin-1-ium tribromide (3a). Light brown oily-waxy solid; Yield 81%; FT-IR (ν/cm^{-1}): 3410 (amide N–H), 3215 (aromatic C–H, pyridinium), 3116 (aromatic C–H, pyridinium), 2938 and 2860 (aliphatic C–H), 1683 (C=O, amide). ^{1}H NMR (600 MHz, DMSO-d_6) (δ, ppm): 9.17 (d, 2H, py–H, ortho), 8.61 (t, 1H, py–H, para), 8.26 (d, 1H, py–H, ortho), 8.16 (t, 2H, py–H, meta), 7.72 (t, 1H, py–H, meta), 7.04 (t, 1H, py–H, para), 6.94 (d, 1H, py–H, meta), 4.63 (t, 2H, py–N^+–C$\underline{H}_2$–CH_2–

$N^+-(CH_3)_3$), 3.34 (s, 9H, $-N^+-(C\underline{H}_3)_3$), 3.15 (t, 2H, py– $N^+-C\underline{H}_2-CH_2-CH_2-$), 2.37 (t, 2H, py–$N^+-CH_2-C\underline{H}_2-N^+-(CH_3)_3$), 2.26 (t, 2H, $-CH_2-C\underline{H}_2-CO-NH$). ^{13}C NMR (150 MHz, DMSO-d_6) δ (ppm): 173.14 ($CH_2-\underline{C}O-NH$), 152.45 ($Py^2-\underline{C}$ para), 148.30 ($Py^2-\underline{C}$ ortho), 145.94 ($Py^1-\underline{C}$ ortho), 145.21 ($Py^1-\underline{C}-NH$), 138.49 ($Py^2-\underline{C}$ meta), 128.50 ($Py^1-\underline{C}$ meta), 119.64 ($Py^1-\underline{C}$ para), 113.82 ($Py^1-\underline{C}$ meta), 60.87 ($Py^2N^+-\underline{C}H_2$), 60.84 ($Py^1N^+-\underline{C}H_2-\underline{C}H_2-N^+-(CH_3)_3$), 60.15 ($Py^1N^+-CH_2-CH_2-N^+-(\underline{C}H_3)_3$), 33.59 ($\underline{C}H_2-CO-NH$), 30.80 ($Py^2N^+-CH_2-\underline{C}H_2$). Anal. Calcd for $C_{21}H_{33}Br_3N_4O$ (MW = 597.22 g/mol): C, 42.23; H, 5.57; N, 9.38. Found: C, 42.08; H, 5.49; N, 9.50.

2.2.2. 2-(4-(1-pyridinium-1-yl)octanamido)-1-2-(trimethylammonio)ethyl)pyridin-1-ium tribromide (3b). Light brown oily-waxy solid; Yield 75%; FT-IR (ν/cm^{-1}): 3391 (amide N–H), 3247 (aromatic C–H, pyridinium), 3127 (aromatic C–H, pyridinium), 2931 and 2858 (aliphatic C–H), 1702 (C=O, amide). ^1H NMR (600 MHz, DMSO-d_6) (δ, ppm): 9.13 (d, 2H, py–H, ortho), 8.60 (t, 1H, py–H, para), 8.26 (d, 1H, py–H, ortho), 8.15 (t, 2H, py–H, meta), 7.72 (t, 1H, py–H, meta), 7.04 (t, 1H, py–H, para), 6.90 (d, 1H, py–H, meta), 4.61 (t, 2H, py–$N^+-C\underline{H}_2-CH_2-N^+-(CH_3)_3$), 3.33 (s, 9H, $-N^+-(C\underline{H}_3)_3$), 3.13 (t, 2H, py–$N^+-C\underline{H}_2-CH_2-CH_2-$), 2.35 (t, 2H, py–$N^+-CH_2-C\underline{H}_2-N^+-(CH_3)_3$), 2.23 (t, 2H, $-CH_2-C\underline{H}_2-CO-NH$). ^{13}C NMR (150 MHz, DMSO-d_6) δ (ppm): 173.28 ($CH_2-\underline{C}O-NH$), 152.52 ($Py^2-\underline{C}$ para), 148.30 ($Py^2-\underline{C}$ ortho), 145.92 ($Py^1-\underline{C}$ ortho), 145.18 ($Py^1-\underline{C}-NH$), 138.48 ($Py^2-\underline{C}$ meta), 128.51 ($Py^1-\underline{C}$ meta), 119.59 ($Py^1-\underline{C}$ para), 113.82 ($Py^1-\underline{C}$ meta), 61.12 ($Py^2N^+-\underline{C}H_2$), 60.09 ($Py^1N^+-\underline{C}H_2-\underline{C}H_2-N^+-(CH_3)_3$), 60.08 ($Py^1N^+-CH_2-CH_2-N^+-(\underline{C}H_3)_3$), 33.86 ($\underline{C}H_2-CO-NH$), 31.09 ($Py^2N^+-CH_2-\underline{C}H_2$). Anal. Calcd for $C_{23}H_{37}Br_3N_4O$ (MW = 625.28 g/mol): C, 44.18; H, 5.96; N, 8.96. Found: C, 44.05; H, 6.09; N, 8.81.

2.3. Determination of Critical Micelle Concentration (CMC)

For the CMC of surfactants determined by the conductometric method using the OHAUS Starter 3100M digital conductivity meter, a step-by-step dilution-extraction method based on specific conductivity measurement was used. In all these processes, the specific conductivity of 30 mL of pure water was determined first, and then 0.5 mL of 10^{-2} M inhibitor solution was added to this water and specific conductivity measurements were carried out after each inhibitor solution added. CMC values were determined from the break point of the curve in the graph of conductivity measurements plotted against inhibitor concentration.

2.4. Surface Tension at CMC

The capillary rise method was employed with a Na-heparinized micro hematocrit tube (BRIS, Soda Lime glass, diameter = 1.0 mm, length = 75 mm, Vitrex Medical, Herlev, Denmark) capillary to assess the surface tensions of aqueous solutions of the tricationic surfactants [38, 39]. The related values were measured at 20°C.

2.5. Foam Properties

To determine the foam height, 25 mL of aqueous solution (at 1×10^{-2} M and at CMC) was stirred brawnily for 10 s in a calibrated 100 mL glass cylinder which has a length of 18 cm and a diameter of 2.2 cm with glass stopper on it. The foam height of the solution was measured after allowing to stand for 30 s [40].

The foam volume variations owing to the swing of the aqueous surfactant solutions (10 mL) at the CMC for 30 s in the same glass cylinder were utilized to determine the foam stability. Foam experiments were carried out at 20°C with ultrapure water. The measurement of foam volume of the surfactant solutions was fulfilled by a sealed glass cylinder which was shaken cogently for 30 s and right after the first measurement was made. In the succeeding stages, the shaken solutions were left for 5 and 30 min before reading the foam volumes [41]. The measurements for each surfactant were repeated twice.

2.6. Emulsion Stability

The mixture of 10 mL surfactant solution and 10 mL mineral oil at the CMC in a 100 mL graduated cylinder with a plastic stopper was used to ascertain the emulsion stability. The glass cylinder was shaken up and down for 30 s at constant rate and then separation time for 9 mL of clean solution was recorded [42].

2.7. Corrosion Tests in 1.0 M HCl

In the corrosion tests carried out in acidic environment, cold rolled steel material with low carbon content was used in accordance with the DIN EN 10130 norm [43]. The composition of the metal plates is 0.07% (C), 0.35% (Mn), 0.015% (P), 0.015% (S) and the rest is Fe.

In corrosion tests based on gravimetric measurements, which were carried out with the method reported in the literature [44], metal plates cut in dimensions of 2.0 × 5.0 cm were kept in 15% HCl solution for 5 min. The aim is to remove the existing rust stains and oxide layers on the metal surface. The surface of the metal plates was washed with distilled water before sanding with emery paper (150). The plates, which were kept in acetone for a while, were first dried in a vacuum oven and then in open air and weighed before the test.

After the tricationic surfactants (**3a–b**) used in the tests were weighed in certain amounts, they were transferred to 100 mL 1.0 M HCl solutions prepared from 37% concentrated hydrochloric acid in order to obtain 25, 50, 100 and 200 ppm solutions in acidic medium. On the other hand, 100 mL of 1.0 M HCl control solution without adding inhibitor was also prepared. Metal plates immersed in acidic solutions with and without inhibitors at room temperature for 24 h were then cleaned with distilled water and acetone and dried. The weight loss in the metal plates, whose mass was also weighed after the test, was calculated.

2.8. Scanning Electron Microscopy (SEM)

Metal plates cut into squares of 0.1 cm thickness, 2.0 cm width and 2.0 cm length were used to obtain SEM images of metal surfaces. After being subjected to corrosion tests in an acidic environment, the metal plates washed with acetone were dried in a vacuum desiccator. Immediately afterwards, SEM images of metal surfaces magnified 1000 times under high vacuum were obtained with a scanning electron microscope (Carl Zeiss EVO 40, Oberkochen, Germany).

2.9. Computational

Our main method of theoretical analysis is the derivation of some descriptors, i.e., chemical potential (μ), chemical hardness (η), and electrophilicity index (ω) with geometry optimizations of the studied structures at the M06-2X/DGDZVP level of theory using Gaussian 09W [45]. All optimizations are reacquired in water using the continuum solvation model SMD [46]. Each descriptor is calculated by the following equations defined within the scope of conceptual DFT;

$$\mu = \left(\frac{\partial E}{\partial N}\right)_{\nu}\left(\underset{r}{\rightarrow}\right) \approx -\frac{(I+A)}{2} = \frac{E_{\mathrm{LUMO}} + E_{\mathrm{HOMO}}}{2} = \chi\,, \quad (1)$$

$$\eta = \left(\frac{\partial^2 E}{\partial N^2}\right)_{\nu}\left(\underset{r}{\rightarrow}\right) = \left(\frac{\partial \mu}{\partial N}\right) x_{\nu}\left(\underset{r}{\rightarrow}\right) = \frac{E_{\mathrm{LUMO}} - E_{\mathrm{HOMO}}}{2}\,, \quad (2)$$

$$S = (2\eta)^{-1} = \frac{1}{(I-A)}, \quad (3)$$

$$\omega = \frac{\mu^2}{2\eta} = \frac{(I+A)^2}{4(I-A)} \approx \frac{(E_{\mathrm{LUMO}} + E_{\mathrm{HOMO}})^2}{4(E_{\mathrm{LUMO}} - E_{\mathrm{HOMO}})}\,, \quad (4)$$

where μ is the electronic chemical potential, E is the total energy, and ν is the external potential. E_{HOMO} signifies the energy of the HOMO, while E_{LUMO} indicates the energy of the LUMO. I and A are the vertical ionization potential and electron affinity of the system respectively, and given as $I = -E_{\mathrm{HOMO}}$ and $A = -E_{\mathrm{LUMO}}$, keeping the external potential fixed [47].

3. RESULTS AND DISCUSSION

3.1. Chemistry

Novel tricationic surfactants were synthesized as potential corrosion inhibitors for mild steel in acidic media. The synthesis pathways of the compounds are shown in Fig. 1. As seen in Fig. 1, synthesis of surfactants containing three cationic groups was carried out in four steps. In the first step, the corresponding ω-bromoalkanoyl chlorides were synthesized from the corresponding ω-bromoalkanoic acids. In the second step, ω-bromo-*N*-(pyridin-2-yl)alkanamide derivatives (**1a–b**) were prepared and in the next step monocationic surfactants (**2a–b**) were obtained. Finally, the tricationic surfactants (**3a–b**) were synthesized as corrosion inhibitor.

The structures of the novel tricationic surfactants were confirmed by FT-IR, ^{1}H NMR and ^{13}C NMR spectroscopic methods. The spectrums of the compounds were given in supplementary material. The IR spectrum of compounds **3a** exhibits intense bands at 3410 and 1683 cm^{-1} due to stretch of amide N-H group and amide carbonyl group (C=O), respectively. Similar stretch values for compound **3b** are 3391, 1702 cm^{-1}. In Experimental section, the characteristic peak values of the surfactants **3a-b** were given. The methylene protons next to pyridine ring N atom have a chemical shift of 4.63 ppm for **3a**, and 4.61 ppm for **3b** as a triplet peak. However, singlet peaks at 3.34 and 3.33 ppm for the nine hidrojen atoms of three methyl groups; triplet peaks at 3.15 and 3.13 ppm for the methylene protons in the long alkyl chain next to pyridine ring N atom and triplet peaks at 2.26 and 2.23 ppm for the methylene protons next to amide carbonyl group are also the basic characteristic peaks of these surfactants. In addition, the evaluation of ^{13}C NMR spectrum of the synthesized corrosion inhibition compounds confirmed their structures. The peaks at 173.14 ppm for **3a** and 173.28 ppm for **3b** belong to C atoms of amide carbonyl groups. The peaks at 60.87 and 61.12 ppm for the methylene protons next to pyridine ring N atom and the peaks at 60.15 and 60.08 ppm for the C atoms of three methyl groups are also the evidence for these synthesized compounds **3a–b**.

3.2. Physicochemical Properties of Surfactants

Density (ρ), critical micelle concentration (CMC), surface tension at CMC (γ_{CMC}), surface effectiveness (π_{CMC}) and Gibbs free energy of micellization (ΔG_{mic}) are ranked among several measured and/or calculated physicochemical parameters. The results are given in Table 1.

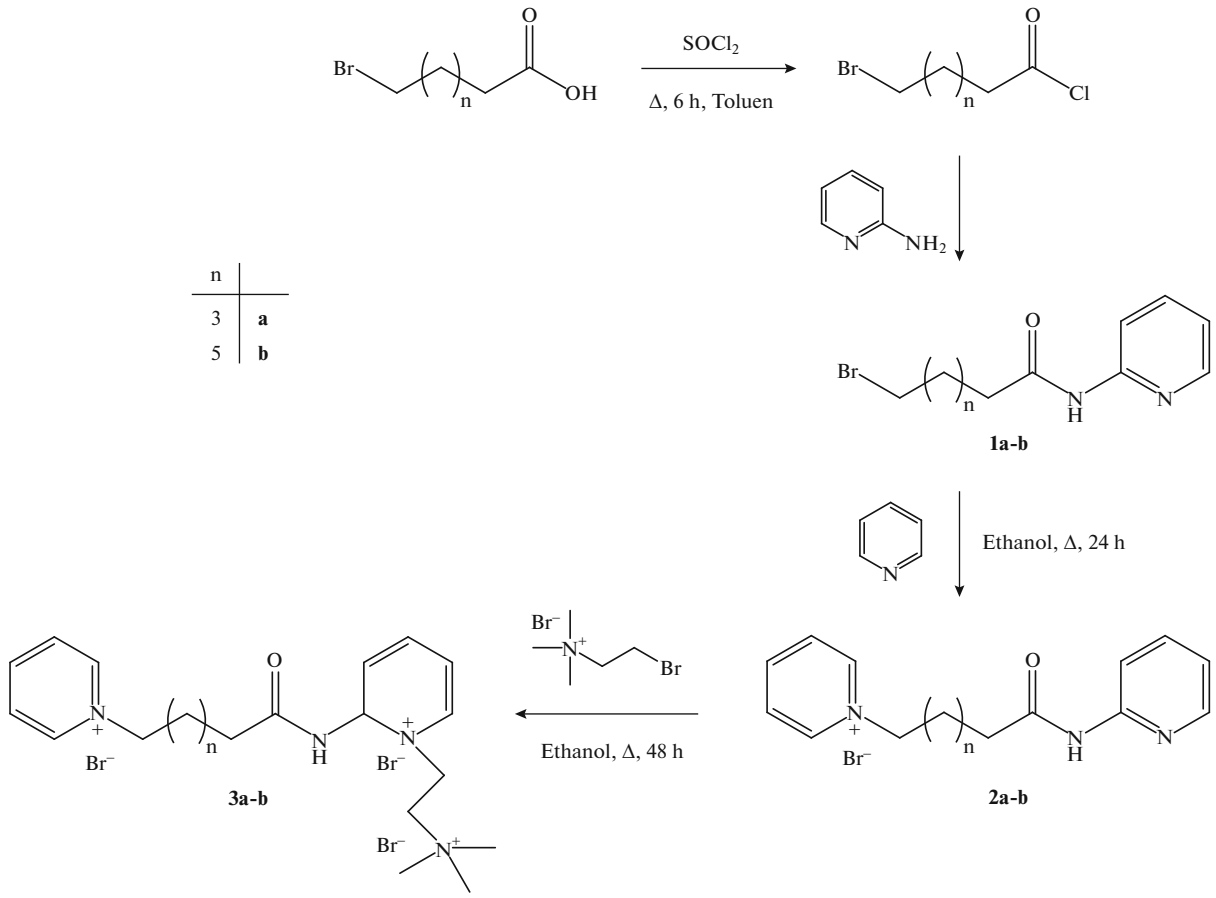


Fig. 1. Synthetic pathways of the tricationic surfactants.

The arrest points in the specific conductivity vs surfactant concentration plots aided to find the CMC values [48] (Fig. 2). A linear increment between conductivity and concentrations was observed as seen in Fig. 2, and the concentration that corresponds to the slope change was designated as critical micelle concentration for the synthesized surfactants. These concentrations were found to be 16.31×10^{-4} M for compound **3a** and 14.97×10^{-4} M for compound **3b**, which point out that the micelles of these cationic surfactants are formed at low concentrations.

The synthesized compounds are not gemini type surfactants. Although the cationic nitrogen groups are the same in the compounds, the only changing point of the surfactants is the long carbon chain. The long chain in compound **3a** has 6 carbons, while the compound **3b** have 8 carbons in the long chain. In the long carbon chain of the compounds, hydrophobicity increases as the number of carbon increases. The greater the hydrophobicity of the surfactant, the greater tendency to form micelles [49]. This affects the critical micelle concentration of the surfactants. As known, the CMC value decreases as the carbon atom numbers increase [50]. The increase of methylene groups in long hydrophobic chains increases the interaction of surfactant molecules. As a matter of fact, this accelerates the micellization of the said compounds even at lower concentrations in solution [51]. Therefore, the CMC value of the compound **3b** was found to be lower than that of **3a**.

Table 1. Physicochemical properties of the cationic surfactants

Compounds	CMC, $\times 10^{-4}$ M[a]	γ_{CMC}, dyn cm^{-1}[a]	π_{CMC}, dyn cm^{-1}	ΔG_{mic}, kj mol^{-1}
3a	16.31	35.29	37.51	−15.64
3b	14.97	32.62	40.18	−15.84

[a] Value measured at 20°C.
[b] Value measured at critical micelle concentration of the surfactant.

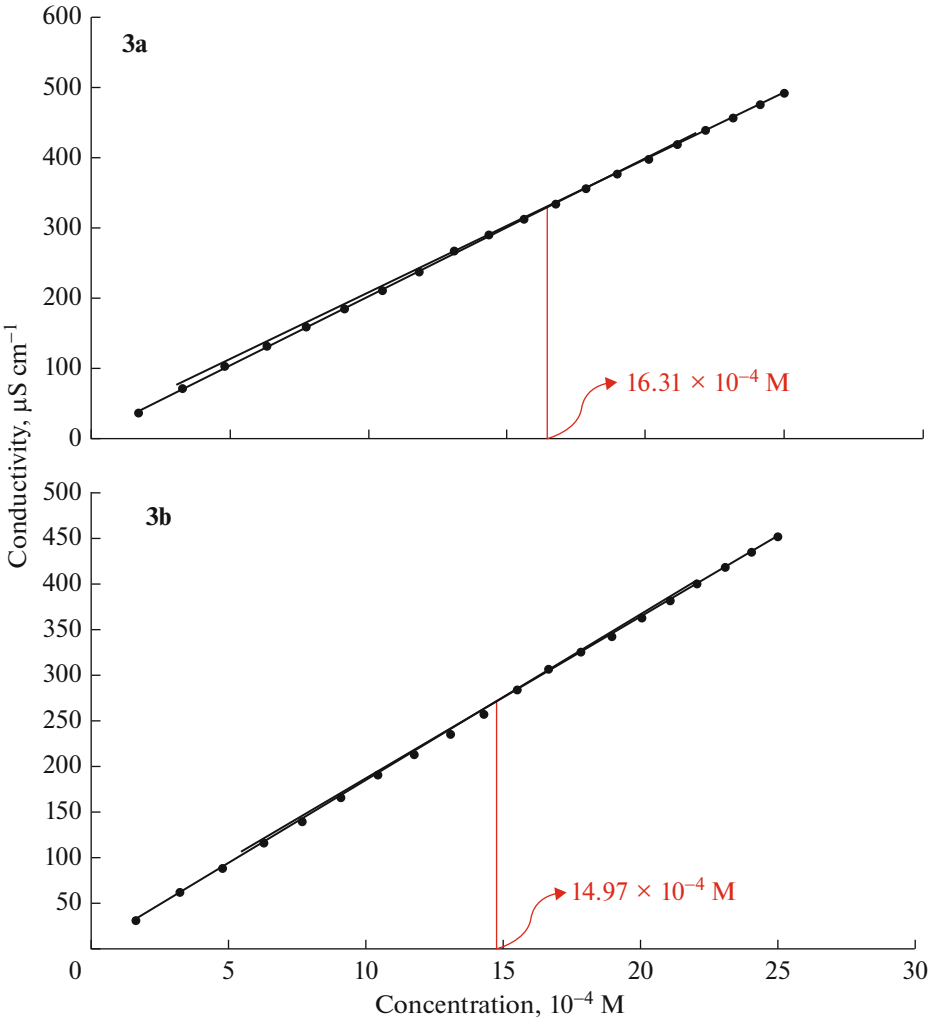


Fig. 2. Graphs of conductivity values measured against concentration.

Surface tensions were tested at the CMC of the surfactants by the capillary rise method [38, 39], which assisted in assessing the surface activity. As seen in Table 1, compound **3b** was found to have lower surface tension. At the CMC of surfactants, the densities detected by 10 mL picometers were quite close to each other. Of these solutions, whose densities in critical micelle concentrations are very close to each other, the surface tension value of the **3b** compound with lower CMC value was also found to be lower.

The maximum reduction of surface tension can be identified by the effectiveness of synthesized surfactant (π_{CMC}) which equals to the difference between surface tension of a pure water and the surface tension of a solution of the surfactant at the CMC. This parameter can be calculated by using the following equation: [29, 52, 53]:

$$\pi_{CMC} = \gamma_0 - \gamma_{CMC}, \quad (5)$$

where γ_0 and γ_{CMC} are the surface tension of pure water (72.8 dyn cm^{-1} at 20°C) and surface tension at CMC, respectively. The effectiveness values were calculated as 37.51 and 40.18 dyn cm^{-1} for the compounds **3a** and **3b**, respectively. As seen Table 1, the π_{CMC} value of the compound **3a**, whose γ_{CMC} value is greater, has been calculated more less. It is known that the lowest value of π_{CMC} belongs to the lowest surface-active analogue [49, 54]. Therefore, the compound **3a** with lower π_{CMC} value will show worse surface activity than the other surfactant.

In addition to this, CMC of the surfactant has an impact on Gibbs free energy of micellization which provides information about the nature of the aggregation process. A decrease in the CMC results in an increase for the tendency of the substance to form micelles. The value of Gibbs free energy of micellization, which is calculated by the following formula, proves this information (Table 1). The negative value

Table 2. Foam height and foam stabilities of the cationic surfactants

Surfactants	Foam height, mm[a] at 1.0×10^{-2} M	Foam height, mm[a] at CMC	Foam volumes, mL[a]									
			initial		after 5 min		after 30 min		Foam stability, % at 1.0×10^{-2} M		Foam stability, % at CMC	
			$(V_0)^b$	$(V_0)^c$	$(V_1)^b$	$(V_1)^c$	$(V_2)^b$	$(V_2)^c$	after 5 min[d]	after 30 min[e]	after 5 min[f]	after 30 min[g]
3a	_[h]	_[h]	_[h]	_[h]	_[h]	_[h]	_[h]	_[h]	_[h]	_[h]	_[h]	_[h]
3b	25	_[h]	7	_[h]	2	_[h]	1	_[h]	28.6	14.3	_[h]	_[h]

[a] Value measured at 20°C.
[b] Foam volume measured at 1.0×10^{-2} M of surfactant concentration.
[c] Foam volume measured at critical micelle concentration of the surfactant.
[d] $[(V_1)^b / (V_0)^b] \times 100$.
[e] $[(V_2)^b / (V_0)^b] \times 100$.
[f] $[(V_1)^c / (V_0)^c] \times 100$.
[g] $[(V_2)^c / (V_0)^c] \times 100$.
[h] no foam formation.

of Gibbs free energy of micellization shows that micelle formation occurs spontaneously.

$$\Delta G_{\text{mic}} = RT \ln(\text{CMC}), \quad (6)$$

ΔG_{mic} is the Gibbs free energy of micellization, R is the ideal gas constant (8.314 J mol^{-1} K^{-1}), T is the absolute temperature (293 K) and CMC is the critical micelle concentration. There are several factors that contribute on micellization process. One of them can be explained for hidrophobic chain. Electrostatic repulsion between heads groups and π–π interaction among the pyridine groups must dominate to favor the micellization. As chain length increases, these interactions are weakened in favor of steric hindrance. Therefore, compound **3b** has a negatively larger ΔG_{mic} value than the other surfactant.

3.3. Foam Height and Foam Stability

Foam height, foam volume and foam stability results were given in Table 2. Foam height was determined for surfactant solutions at 1.0×10^{-2} M and at the CMC. Foam volumes and foamstabilities were measured for 1.0×10^{-2} M and for CMC at different times (5 and 30 min) [41]. As seen in Table 2, the two cationic surfactants did not form foam at the CMC. The fact that they do not form foam at low concentrations is compatible with the knowledge that cationic surfactant compounds do not form a pronounced foam [42]. It is also known that the foamability decreases as the concentration decreases due to micellar stability [41]. When the foam stability of cationic surfactants at 1.0×10^{-2} M concentration was compared, it was found that there was no foam stability for **3a**, because compound **3a** could not form foam; however, it appears to exhibit little foam stability for compound **3b**. As a reason for this result, we can say that compound **3b** has a better hydrophobic character.

3.4. Emulsion Stability

Table 3 shows the results of emulsion stability of the synthesized tricationic surfactant at 1.0×10^{-2} M and at CMC concentrations. As can be seen, the emulsion stabilities were performed at 20°C and the separation times of mineral oil-water were measured in seconds time unit. It is known that emulsion power increases as the separation time increases [55]. Both cationic surfactants showed greater emulsion stability at a concentration of 1.0×10^{-2} M. The emulsion stability has changed with the carbon chain length of the cationic surfactant. At both concentrations, the **3b** compound containing the longer carbon chain showed the greatest emulsion stability. Compound **3a**, which has the lower carbon number in the long carbon chain, showed a lower emulsion power.

3.5. Anticorrosion Properties of Tricationic Surfactants in Acidic Medium

Inhibition efficiencies measured at different concentrations of surfactants according to weight loss are given in Table 4. Corrosion tests using 1.0 M HCl solution as corrosive medium were carried out for 24 h at room temperature. Corrosion inhibition activities are calculated with the following formula:

$$IE\ \% = \frac{Wo - W}{Wo} \times 100\ , \quad (7)$$

where ($IE\%$) is the percentage inhibition efficiency, Wo is the weight loss of the coupon in the absence of an inhibitor, and W is the weight loss of the coupon in the same environment in the presence of an inhibitor. Table 4 shows that as the inhibitor concentration increases for all surfactants, inhibition activities also increase. This is an expected result. Because, it is known that surfactants have increased activity against corrosion with the increase of inhibitor concentration

Table 3. Emulsion stabilities of the synthesized cationic surfactants[a]

Surfactants	Emulsion stability (s) at 1.0×10^{-2} M (ES_1)	Emulsion stability (s) at CMC (ES_2)
3a	21	19
3b	109	30

[a]Value measured at 20°C.

Table 4. Corrosion inhibition efficiencies (IE %) which is calculated for different concentrations of the surfactants in 1.0 M HCl medium for 24 h at room temperature (weight loss method)

Surfactants	Corrosion inhibition efficiencies, IE %			
	25 ppm	50 ppm	100 ppm	200 ppm
3a	62.07	68.63	76.05	76.24
3b	84.98	88.02	90.87	92.97

[14, 17, 29, 30, 32, 56–58]. On the other hand, in each concentration value studied, it was found that the inhibition efficiency of the **3b** compound containing longer carbon chain was heigher. In the **3a** compound containing a shorter carbon chain, inhibition activities were determined to be lower. The reason for this situation is, as expected, the inhibition efficiency increases as the carbon chain increases in the surfactant [34, 35, 59–62].

3.6. Corrosion Inhibition Mechanism

Corrosion inhibition is thought to be caused by the adsorption of the inhibitor onto the metal surface and thus by blocking the active regions of the carbon steel surface. When we compare the structures of the synthesized tricationic surfactants, the only structure difference in the substances is the number of carbons in the hydrophobic long chain. Other parts of the compounds in their chemical structure are the same. As can be seen in the adsorption mechanism given in the Fig. 3, the metal surface, which is positively charged as a result of the oxidation of iron to +2 oxidation step in the anode reaction of the corrosion phenomenon, turned into negative by forming a dipole with the effect of chloride ions from the acid [34, 62]. To the negatively charged dipole, the positively charged nitrogen atoms of the inhibitors are adsorbed on the metal surface by electrostatic interaction. In addition, unpaired electron pairs of the oxygen atom in the carbonyl group and π electrons in the aromatic pyridine ring, which are in the structure of the compounds, interact with the empty d orbitals of the Fe element in the metal plates and adhere to the metal surface chemically. The negative effect of the acidic corrosive environment on the metal surface is prevented by both chemical and physical adsorption (Fig. 3).

3.7. SEM

The metal surface images obtained by scanning electron microscope are given in Fig. 4. Figure 4a is the image of metal surface immersed in 1.0 M HCl solution in inhibitor-free medium for 24 h, while Figs. 4b and 4c are metal surfaces immersed in acid solution containing inhibitor. Figures 4b and 4c are images of metal surfaces immersed in acidic media containing 100 ppm inhibitors **3a** and **3b**, respectively. As can be seen in Fig. 4, it is possible to clearly see the roughness and corrosion products on the metal surface, since the image A belongs to the environment without inhibitor. In contrast, deposits of corrosion products were not observed in the images of the metal surface (Figs. 4b and 4c) immersed in acid solutions with 100 ppm inhibitor. This result shows that metal surfaces immersed in acid solution containing inhibitor are protected against acid-induced corrosion. The scratch marks seen in Figs. 4b and 4c are due to sanding of metal surfaces.

3.8. Quantum Chemistry Calculations

The optimized molecules of **3a** and **3b** are shown in Fig. 5. In general, the prediction of the inhibition behavior of electronic systems rests upon the capability to assess an important property, namely the global reactivity. The HOMO and the LUMO are loadstars to perceive chemical reactivity. E_{HOMO} and E_{LUMO} fill electron donor's and electron acceptor's boots, respectively. Hence, lower is the energy gap (ΔE); better is the electron transfer process. Figure 6 shows the shapes of HOMO and LUMO for the investigated molecules. It is discovered from this figure that the HOMO of **3a** is mainly distributed on the Br atoms, whereas the LUMO is localized on the C and N atoms of pyridine ring. On the other hand, the HOMO is interspersed between carbon chain and Br ion, and the LUMO is apportioned over the longitudinal pyridine

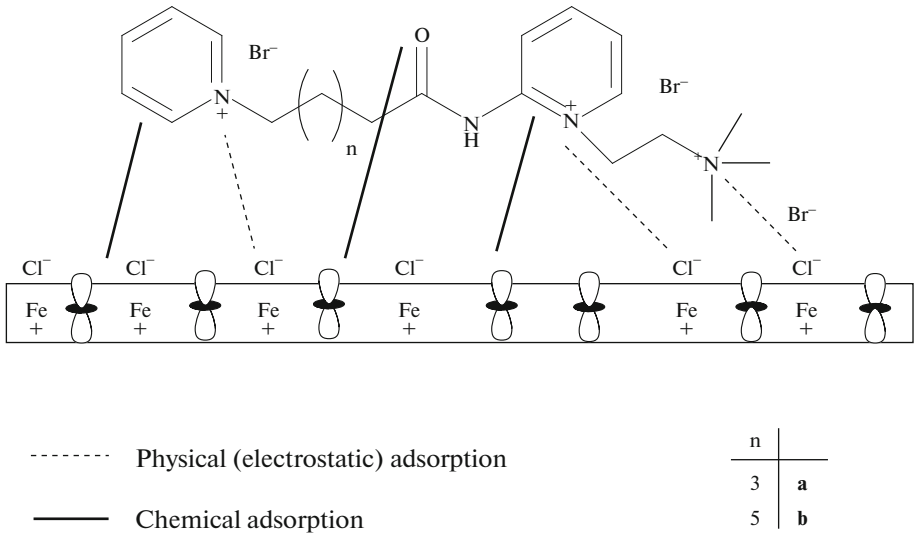


Fig. 3. Adsorption mechanism of tricationic surfactans on the metal surface.

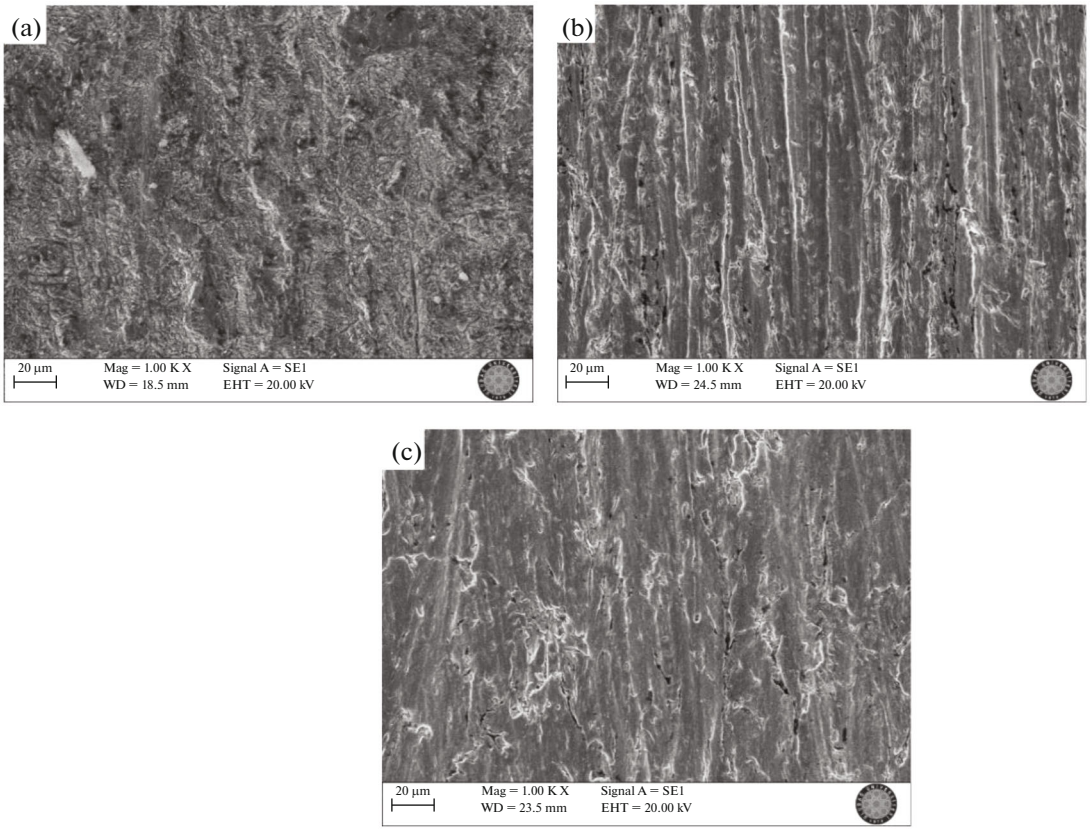


Fig. 4. SEM images of metal surfaces. (a) 1.0 M HCl without inhibitor; (b) 1.0 M HCl containing 100 ppm of compound **3a**; (c) 1.0 M HCl containing 100 ppm of compound **3b.**

moiety as well as N atoms of secondary and tertiary amine groups of **3b** molecule.

Table 5 lists the computed parameters. As is evident, **3a** has the highest E_{HOMO} and the lowest E_{LUMO} and ΔE values in aqueous phase compared to those of **3b**. Dipole moment ($\partial(D)$) of the compound, despite its relation being controversial, is another parameter which makes a guess for the polarized nature. The growth in the total dipole moment is generally slated for an increased inhibitor efficiency [36], and the data

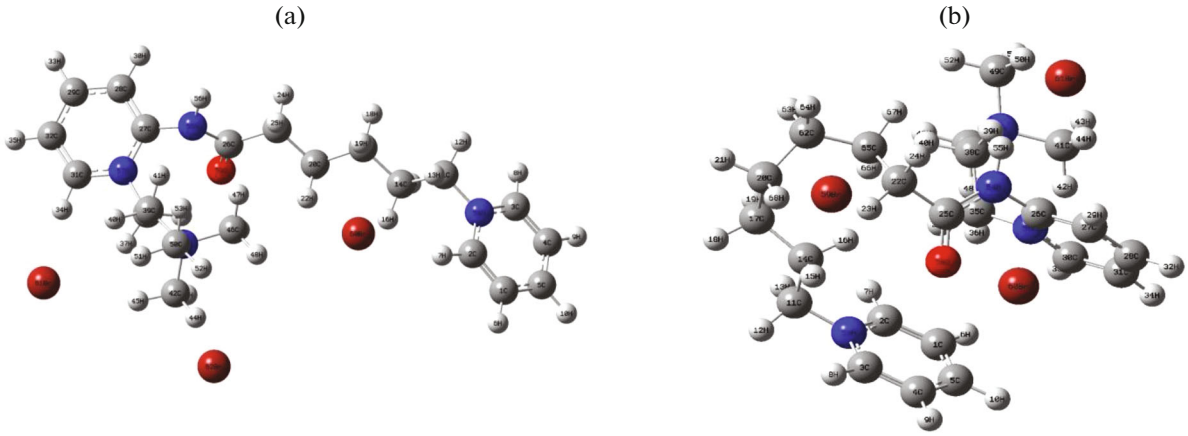


Fig. 5. Optimized structure of (a) **3a** and (b) **3b** in aqueous phase at the M06-2X/DGDZVP level.

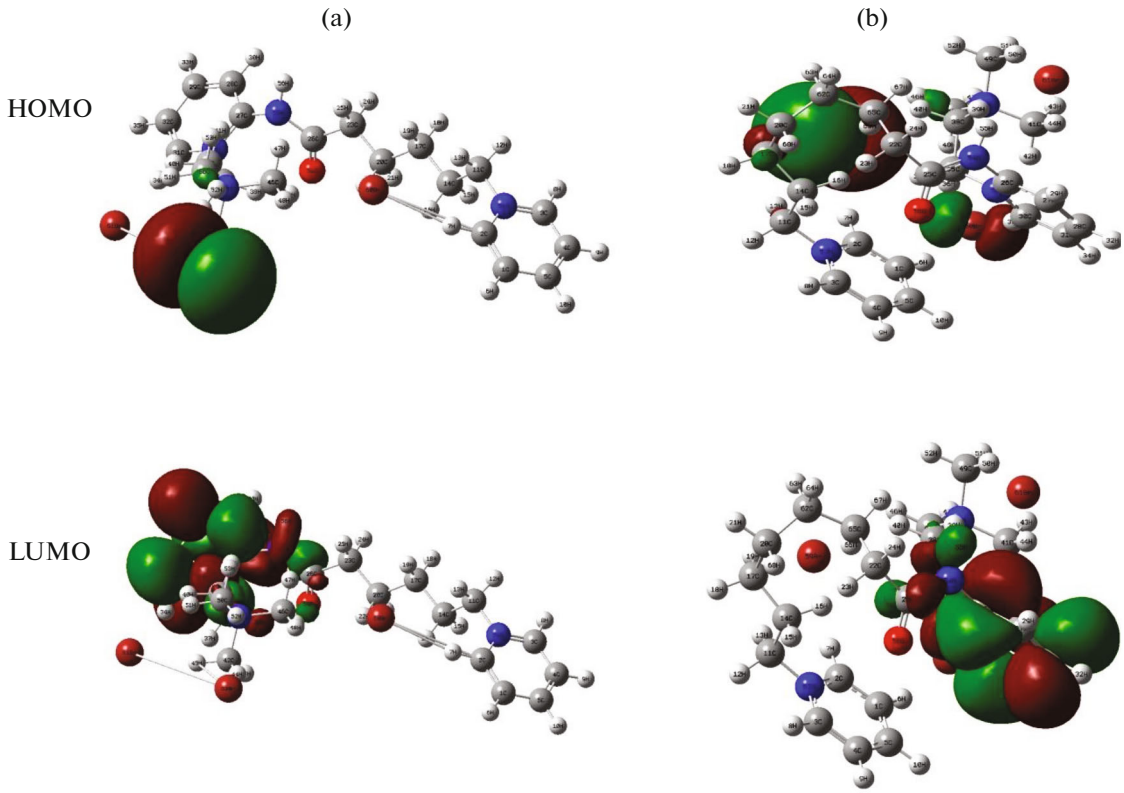


Fig. 6. Plots of HOMO and LUMO orbital distribution for (a) **3a** and (b) **3b.**

has shown that **3a** has a higher value of dipole moment than **3b**. A lower value of ω spells for an actuose nucleophile, conversely a higher value of ω spells for a decent electrophile. Concordantly, **3a** seems to behave as a nucleophile, whereas **3b** has a role of an electrophile. The energy disparity is large and small for a hard and a soft molecule, respectively. Due to their nature of easy electron acceptance soft molecules are more reactive compared to the hard ones. As one can see, **3a** is softer than **3b**. The comparison of η values also shows a similar trend to those of the energy gaps, with **3a** being the lowest. In essence, no simple relation with the inhibition performance of these inhibitors could be established. This is not surprising because feedback from experimental validation to computed quantum chemical parameters of the compounds can be complicated by subtle yet important differences between compounds synthesized in the laboratory compared to the ideality of repesentative structural models on a computer. Such conclusions were also ratified and expatiated by other computational corrosion studies [63, 64].

Table 5. Molecular electronic parameters of (a) **3a** and (b) **3b**

Parameters	**3a**	**3b**
E_{HOMO}, eV	−6.712	−7.128
$E_{LUMO,}$ eV	−1.415	−1.414
ΔE (E_L−E_H), eV	5.297	5.714
∂, D	50.791	15.568
ω	3.117	3.192
χ	4.064	4.271
η	2.649	2.857
S	0.189	0.175
E_T, eV	−240416.280	−242555.342

4. CONCLUSIONS

Thanks quaternization reactions, two tricationic surfactants containing two positively charged pyridine nitrogens and one positively charged quaternary ammonium nitrogen were synthesized. The critical micelle concentrations of tricationic surfactants and the surface tensions at this concentration (γ_{CMC}) were determined. As a result of the findings, it was observed that the CMC and surface tension values at this concentration decreased as the long carbon chain in surfactants increased. The micelle formation free energy value of the **3b** compound with the higher number of carbons in its long chain was found to be higher in the negative direction. This shows that compound **3b** releases more energy during micelle formation. It was observed that compound **3b** could form foam in 1.0×10^{-2} M aqueous solutions, while compound **3a** could not. It was observed that both tricationic surfactants could not form foam at their critical micelle concentrations. It has been found that as the carbon chain length increases in tricationic surfactants, the emulsion stability also increases. As a result of the corrosion tests performed using the weight loss method, it was determined that the increase in the inhibition activities was achieved with the increase in the concentration of each synthesized surfactant inhibitor in the solution. When the surfactants were compared with each other in terms of inhibitor effectiveness values, the following ranking was obtained in corrosion inhibitor activity: **3b** > **3a**. As the reason for this result, we can show that the inhibition efficiency increases as the carbon chain length increases in surfactants that dissolve well in water. As a result of DFT analysis, it seems that no cohorent picture has emerged about the inhibition behaviour of the surfactants calling for a comprehensive theoretical study to be performed at the solid/water interface if a method can be found in the future that does not suffer from accuracy and realibility problems.

FUNDING

We thank Bursa Uludağ University Scientific Research Projects Unit for providing financial support to this study under the Project Number: OUAP(F)-2019/15.

CONFLICT OF INTEREST

The authors of this work declare that they have no conflicts of interest.

SUPPLEMENTARY INFORMATION

The supporting information includes the FT-IR, ^{1}H NMR and ^{13}C NMR spectrums of the compounds (**3a–b**).

The online version contains supplementary material available at https://doi.org/10.1134/S2070205123700673.

REFERENCES

1. Berger, D.M., *Corrosion Theory,* Gilbert/Commonwealth Co., 1990, p. 308.
2. Aydoğdu, E., *MSc Thesis,* Adana: Institute of Naturel and Applied Sciences, Univ. of Çukurova, 2010.
3. Bilgic, S., *Corrosion,* 2008, vol. 16, p. 3.
4. Revie, R.W. and Uhlig, H.H., *An Introduction to Corrosion Science and Engineering,* Hoboken, NJ: John Wiley and Sons, 2008, p. 2.
5. Prawoto, Y., Ibrahim, K., and Wan Nik, W.B., *Arabian J. Sci. Eng.,* 2009, vol. 34, p. 115.
6. Eliassen, R., Pereda, C., Romeo, A.J., and Skrinde, R.T., *J. AWWA,* 1956, vol. 48, p. 1005.
7. Li, X., Deng, S., and Fu, H., *Prog. Org. Coat.,* 2010, vol. 67, p. 420.
8. Tizpar, A. and Ghasemi, Z., *Appl. Surf. Sci.,* 2006, vol. 252, p. 8630.
9. Tebbji, K., Hammouti, B., Oudda, H., Ramdani, A., and Benkadour, M., *Appl. Surf. Sci.,* 2005, vol. 252, p. 1378.
10. Üneri, S., *Korozyon ve Önlenmesi. Segem,* Ankara, 1998, p. 413.
11. Gabler, C., Tomastik, C., Brenner, J., Pisarova, L., Doerr, N., and Allmaier, G., *Green Chem.,* 2011, vol. 13, p. 2869.
12. Monnier, J., Réguer, S., Foy, E., Testemale, D., Mirambet, F., Saheb, M., Dillmann, P., and Guillot, I., *Corros. Sci.,* 2014, vol. 78, p. 293.
13. Goyal, M., Kumar, S., Bahadur, I., Verma, C., and Ebenso, E.E., *J. Mol. Liq.,* 2018, vol. 256, p. 565.

14. Malik, M.A., Hashim, M.A., Nabi, F., AL-Thabaiti, S.A., and Khan, Z., *Int. J. Electrochem. Sci.,* 2011, vol. 6, p. 1927.

15. Tanford, C., *Structures in an Aqueous World: The Hydrophobic Effect. Formation of Micelles and Biological Membranes,* New York: Wiley-Interscience, 1973.

16. Mobin, M., Aslam, R., Zehra, S., and Ahmad, M., *J. Surfactants Deterg.,* 2017, vol. 20, p. 57.

17. Hegazy, M.A., Abdallah, M., and Ahmed, H., *Corros. Sci.,* 2010, vol. 52, p. 2897.

18. Sun, Y.M. and Chen, H.L., *Adv. Mater. Res.,* 2012, vol. 427, p. 3.

19. Haque, J., Srivastava, V., Verma, C., Lgaz, H., Salghic, R., and Quraishi, M.A., *New J. Chem.,* 2017, vol. 41, p. 13647.

20. Hegazy, M.A., Ahmed, H.M., and El-Tabei, A.S., *Corros. Sci.,* 2011, vol. 53, p. 671.

21. Hegazy, M.A., Badawi, A.M., Abd El Rehim, S.S., and Kamel, W.M., *Corros. Sci.,* 2013, vol. 69, p. 110.

22. Abdallah, M., Eltass, H.M., Hegazy, M.A., and Ahmed, H., *Prot. Met. Phys. Chem. Surf.,* 2016, vol. 52, p. 721.

23. Abd El-Lateef, H.M., Soliman, K.A., and Tantawy, A.H., *J. Mol. Liq.,* 2017, vol. 232, p. 478.

24. Kaczerewska, O., Leiva-Garcia, R., Akid, R., Brycki, B., Kowalczyk, I., and Pospieszny, T., *J. Mol. Liq.,* 2018, vol. 249, p. 1113.

25. Abdallah, M., Hegazy, M.A., Alfakeer, M., and Ahmed, H., *Green Chem. Lett. Rev.,* 2018, vol. 11, p. 457.

26. Öztürk, S., *Russ. J. Org. Chem.,* 2019, vol. 55, p. 245.

27. Pakiet, M., Kowalczyk, I., Garcia, R.L., Akid, R., and Brycki, B., *J. Mol. Liq.,* 2020, vol. 315, p. 113675.

28. El Basiony, N.M., Badr, E.E., Baker, S.A., and El-Tabei, A.S., *Appl. Surf. Sci.,* 2021, vol. 539, p. 148246.

29. El-Tabei, A.S., Hegazy, M.A., Bedair, A.H., and Sadeq, M.A., *J. Surfactants Deterg.,* 2014, vol. 17, p. 341.

30. Bensajjay, F., Alehyen, S., El Achouri, M., Hajjaji, N., Bellaouchou, A., Perez, L., and Infante, M.R., *Anti-Corros. Methods Mater.,* 2011, vol. 58, p. 258.

31. El-Said, W.A., Moharram, A.S., Hussein, E.M., and El-Khawaga, A.M., *J. Surfactants Deterg.,* 2018, vol. 21, p. 343.

32. Eldougdoug, W.I., Ali, A.I., Elaraby, A., and Mabrouk, E.M., *J. Basic Environ. Sci.,* 2018, vol. 5, p. 289.

33. Öztürk, S., Özkazanlı, M.M., Akyıldız, I., Kara, T., and Çelik, F., *Avrupa Bilim ve Teknoloji Dergisi,* 2021, vol. 21, p. 669.

34. Yıldırım, A., Öztürk, S., and Çetin, M., *J. Surfactants Deterg.,* 2013, vol. 16, p. 13.

35. Öztürk, S., Yıldırım, A., Çetin, M., and Tavaslı, M., *J. Surfactants Deterg.,* 2014, vol 17, p. 471.

36. Gece, G., *Corros. Sci.,* 2008, vol. 50, p. 2981.

37. Taylor, C.D., Kurapati, Y., and Mondal, S.K., *Metals,* 2018, vol. 8, p. 81.

38. Sugden, S., *J. Chem. Soc., Trans.,* 1921, vol. 119, p. 1483.

39. Martino, W., Fernandez de la Mora, J., Yoshida, Y., Saito, G., and Wilkes, J., *Green Chem.,* 2006, vol. 8, p. 390.

40. El-Sukkary, M.A., El-Sawy, A.A., and El-Dib, F., *Hung. J. Ind. Chem.,* 1987, vol. 15, p. 317.

41. Kuliszewska, E. and Brecker, L., *J. Surfactants Deterg.,* 2014, vol. 17, p. 951.

42. Negm, N.A. and Mohamed, A.S., *J. Surfactants Deterg.,* 2004, vol. 7, p. 23.

43. Standard EN 10130:2006, German version DIN (Deutsches Institut für Normung e.V.), 2007.

44. Öztürk, S., *Prot. Met. Phys. Chem. Surf.,* 2018, vol. 54, p. 953.

45. Frisch, M.J., Trucks, G.W., Schlegel, H.B., Scuseria, G.E., Robb, M.A., Cheeseman, J.R.,Scalmani, G., Barone, V., Mennucci, B., Petersson, G.A., Nakatsuji, H., Caricato, M., Li, X.,Hratchian, H.P., Izmaylov, A.F., Bloino, J., Zheng, G., Sonnenberg, J.L., Hada, M., Ehara, M., Toyota, K., Fukuda, R., Hasegawa, J., Ishida, M., Nakajima, T., Honda, Y., Kitao, O., Nakai, H.,Vreven, T., Montgomery, J.A., Jr., Peralta, J.E., Ogliaro, F., Bearpark, M., Heyd, J.J., Brothers,E., Kudin, K.N., Staroverov, V.N., Kobayashi, R., Normand, J., Raghavachari, K., Rendell, A., Burant, J.C., Iyengar, S.S., Tomasi, J., Cossi, M., Rega, N., Millam, J.M., Klene, M., Knox, J.E., Cross, J.B., Bakken, V., Adamo, C., Jaramillo, J., Gomperts, R., Stratmann, R.E., Yazyev, O., Austin, A.J., Cammi, R., Pomelli, C., Ochterski, J.W., Martin, R.L., Morokuma, K., Zakrzewski,V.G., Voth, G.A., Salvador, P., Dannenberg, J.J., Dapprich, S., Daniels, A.D., Farkas, Ö., Foresman, J.B., Ortiz, J.V., Cioslowski, J., and Fox, D.J., *Gaussian 09, Revision C.01,* Wallingford, CT: Gaussian Inc., 2009.

46. Marenich, A.V., Cramer, C.J., and Truhlar, D.G., *J. Phys. Chem. B,* 2009, vol. 113, p. 6378.

47. Diaz-Ballote, L., Maldonado-Lopez, L., San-Pedro, L., Hernández-Nuñez, E., and Genesca, J., *J. Serb. Chem. Soc.,* 2022, vol. 87, p. 1.

48. Tyagi, P. and Tyagi, R., *Eur. J. Lipid Sci. Technol.,* 2011, vol. 113, p. 848.

49. Verma, S.K. and Ghosh, K.K., *J. Surfactants Deterg.,* 2011, vol. 14, p. 347.

50. Zana, R., *J. Colloid Interface Sci.,* 2002, vol. 246, p. 182.

51. Negm, N.A., Migahed, M.A., Farag, R.K., Fadda, A.A., Awad, M.K., and Shaban, M.M., *J. Mol. Liq.,* 2018, vol. 262, p. 363.

52. El-Tabei, A.S. and Hegazy, M.A., *J. Surfactants Deterg.,* 2013, vol. 16, p. 757.

53. Öztürk, S., Yıldırım, A., Gece, G., and Türkdemir, H., *J. Surfactants Deterg.,* 2019, vol. 22, p. 197.

54. Tawfik, S.M., Abd-Elaal, A.A., Shaban, S.M., and Roshdy, A.A., *J. Ind. Eng. Chem.,* 2015, vol. 30, p. 112.

55. Bao, Y., Guo, J., Ma, J., Li, M., and Li, X., *J. Mol. Liq.,* 2017, vol. 242, p. 8.

56. Al-Sabagh, A.M., Kandil, N.G., Ramadan, O., Amer, N.M., Mansour, R., and Khamis, E.A., *Egypt. J. Pet.,* 2011, vol. 20, p. 47.

57. Hegazy, M.A., El-Tabei, A.S., Bedair, A.H., and Sadeq, M.A., *RSC Adv.,* 2015, vol. 5, p. 64633.

58. Feng, L., Yin, C., Zhang, H., Li, Y., Song, X., Chen, Q., and Liu, H., *ACS Omega,* 2018, vol. 3, p. 18990.

59. Mobin, M. and Masroor, S., *Int. J. Electrochem. Sci.,* 2012, vol. 7, p. 6920.

60. Hegazy, M.A., Abd El-Rehim, S.S., Badr, E.A., Kamel, W.M., and Youssif, A.H., *J. Surfactants Deterg.,* 2015, vol. 18, p. 1033.

61. Tawfik, S.M., Abd-Elaal, A.A., and Aiad, I., *Res. Chem. Intermed.,* 2016, vol. 42, p. 1101.

62. Öztürk, S., *Prot. Met. Phys. Chem. Surf.,* 2017, vol. 53, p. 920.

63. Kokalj, A., Lozinšek, M., Kapun, B., Taheri, P., Neupane, S., Losada-Pérez, P., Xie, C., Stavber, S., Crespo, D., Renner, F.U., Mol, A., and Milošev, I., *Corros. Sci.,* 2021, vol. 179, p. 108856.

64. Kokalj, A., *Corros Sci.,* 2021, vol. 180, p. 109016.